Planet. Space Sci., Vol. 35, No. 11, pp. 1405–1418, 1987
Printed in Great Britain.

0032-0633/87 $3.00+0.00

DEPENDENCE OF THE REGION II FIELD-ALIGNED CURRENTS ON IONOSPHERIC CONDUCTIVITY GRADIENTS

Q. C. CHENG, J. R. KAN and S.-I. AKASOFU
Geophysical Institute, University of Alaska, Fairbanks, AK 99775-0800, U.S.A.

(*Received* 25 *May* 1987)

Abstract—The effect of the ionospheric conductivity distribution on the field-aligned currents in the polar ionosphere is systematically studied. It is shown that the intensity and the location of the Region II field-aligned current in the magnetosphere–ionosphere coupling are critically dependent on the latitudinal gradient of the Pedersen conductivity in the morning and afternoon sectors around the auroral oval. Moreover, the Region II current density is also found to increase as the conductance ratio Σ_H/Σ_P is reduced by increasing Σ_P.

1. INTRODUCTION

Field-aligned currents play an important role in the magnetosphere–ionosphere (M–I) coupling. The existence of such currents was first suggested by Birkeland around the turn of the century and revitalized by Alfvén in 1939. Satellite measurements showed a broad region of field-aligned currents above the auroral oval (Zmuda and Armstrong, 1974; Iijima and Potemra, 1978; Sugiura and Potemra, 1976). The latitudinal width of this large-scale field-aligned current system is of a few hundred kilometers. Iijima and Potemra (1978) designated the poleward part and equatorward part of the field-aligned current system as the Region I and Region II field-aligned currents, respectively. In the afternoon sector, the Region I field-aligned current flows upward while the Region II downward; the sense is reversed in the morning sector. The magnitude of the Region I current density during quiet condition is less than 1.6 μA m^{-2}. During active periods upward field-aligned current can be as high as 10 μA m^{-2} at the head of the Westward Traveling Surge. The density in the Region II field-aligned current is about half of the Region I current density (Iijima and Potemra, 1978). Embedded in the Region I and Region II currents are thin but intense current sheets (Sugiura *et al.*, 1984).

In the magnetosphere–ionosphere coupling process the conductive ionosphere acts as a variable load. The spatial and temporal variability of the ionospheric conductance affects the closure of the field-aligned currents which in turn produces feedback effects on the magnetospheric convection. The purpose of this paper is to present the results of a systematic quantitative study of the dependence of the Region II field-aligned current on the conductivity distribution in the magnetosphere–ionosphere coupling. The study is based on a self-consistent M–I coupling model in which the Alfvén waves are responsible for the temporal evolution of the field-aligned currents and the convection electric field. It will be shown that the Region II field-aligned currents depend critically on the latitudinal gradient of the ionospheric conductance and to a lesser degree on the conductance ratio Σ_P/Σ_H.

2. REGION II CURRENTS IN THE MAGNETOSPHERE–IONOSPHERE COUPLING

In this section, we calculate the dependence of the Region II field-aligned currents on the ionospheric conductance and the convection pattern from a self-consistent M–I coupling model (Kan and Sun, 1985). The basic idea of this M–I coupling model can be summarized as follows. An enhancement of the magnetospheric convection electric field launches Alfvén waves which propagate toward the conjugate ionospheres along field lines. The ionospheric convection pattern and the current system evolve as the Alfvén waves bounce in the model on the Alfvén transit time scale ($\sim$2–4 min). This time scale is short compared with the substorm time scale ($\sim$30–60 min).

The reflection of Alfvén waves from the ionosphere is determined by equating the field-aligned current behind the incident and reflected Alfvén waves to the divergence of the ionospheric current. The result is given by (Kan and Sun, 1985)

$$(\Sigma_A+\Sigma_P)\nabla\cdot\mathbf{E}^r+(\nabla\Sigma_P-\hat{\mathbf{B}}_0\times\nabla\Sigma_H)\cdot\mathbf{E}^r = (\Sigma_A-\Sigma_P)\nabla\cdot\mathbf{E}^i-(\nabla\Sigma_P-\hat{\mathbf{B}}_0\times\nabla\Sigma_H)\cdot\mathbf{E}^i \quad (1)$$

where $\Sigma_A = 1/(\mu_0 V_A)$ is the characteristic conductance of the plasma in the Alfvén wave, $\mathbf{E}^i$ and $\mathbf{E}^r$ are the electric fields of the incident and reflected Alfvén waves, respectively, and $\hat{\mathbf{B}}_0$ is the unit vector of the magnetic field in the ionosphere.

The physics governing the reflection of Alfvén waves from the magnetospheric boundaries can be summarized as follows (Kan and Sun, 1985). On open field lines the solar wind inertia is sufficiently large so that the $\mathbf{E} \times \mathbf{B}$ flow in the solar wind is either unaffected or only slightly modified by the incident Alfvén waves at the magnetopause. It follows that the $\mathbf{E}$ field on open field lines at the magnetopause is kept more or less constant by the solar wind. Thus, $R_m(E) = E^r/E^i \simeq -1$. The situation on closed field lines is quite different. The inertia of the $\mathbf{E} \times \mathbf{B}$ convection in the plasma sheet is limited and therefore can be modified by the incident Alfvén waves. If the inertia in the plasma sheet is sufficiently small, then an Alfvén wave incident on the plasma sheet will be transmitted almost without reflection. If the conjugate ionospheres are identical, the two transmitted waves at the plasma sheet from opposite hemispheres will be almost identical. By regarding the transmitted waves as if they were reflected, the equivalent reflection coefficient is $R_m(E) \simeq +1$. On the other hand, if the inertia of the plasma sheet is sufficiently large, $R_m(E) \simeq -1$. In summary, one can expect

$$\begin{aligned} R_m(E) &\simeq -1 \quad \text{on open field lines} \\ -1 \leqslant R_m(E) &\leqslant +1 \quad \text{on closed field lines} \end{aligned} \tag{2}$$

where the value of $R_m(E)$ on closed field lines is likely to increase from -1 to $+1$ as one moves from distant tail field lines toward the inner edge of the plasma sheet.

The ionospheric conductivity is enhanced by the precipitation of auroral electrons. Kan and Kamide (1985) presented a conductivity enhancement model based on balancing the ionization produced by discrete auroral precipitations with the recombination in a steady state, i.e.

$$\begin{aligned} \Sigma_H &= \Sigma_0 \quad J_\parallel < J_0 \\ \Sigma_H &= \Sigma_0 \quad J_\parallel > J_0 \nabla \cdot \mathbf{E} \geqslant 0 \\ \Sigma_H &= \Sigma \quad J_\parallel > J_0 \nabla \cdot \mathbf{E} < 0 \end{aligned} \tag{3}$$

where

$$\begin{aligned} \Sigma &= [\Sigma_0^2 + \gamma J'(J' - J_0)]^{1/2} \\ J' &= J_\parallel \quad J_\parallel < J_c \\ J' &= J_c \quad J_\parallel > J_c \end{aligned}$$

and Σ_0 is the background ionospheric conductivity, $J_\parallel$ is the field-aligned current, J is the flux-limited saturation current, J_0 is the current carried by thermal electrons in the loss cone and γ is a parameter depending on the ionization and recombination rates. In all our cases, we choose $J_0 = 0.08$ μA m^{-2}, $J_c = 0.8$ μA m^{-2} and $\gamma = 300$ (mho μA^{-1})^2.

The input parameters are (1) the magnetospheric convection, (2) the distribution of magnetospheric reflection coefficient and (3) the background ionospheric conductivity distribution due to solar e.u.v. and diffuse auroral precipitations. The temporal evolution of the convection pattern, the electrojet currents, the field-aligned currents and the ionospheric conductivity can be calculated by solving equation (1) for $\mathbf{E}^r$ to update $\mathbf{E}$ and J and using equation (3) to update the conductivity as has been described in detail by Kan and Sun (1985). For comparison, we denote the conductivity model studied by Kan and Sun (1985) as case 1. The 10 conductivity models studied in the present paper are enumerated as cases 2–11.

In each case the background ionospheric conductivity consists of the solar e.u.v. ionization and the ionization due to the diffuse auroral precipitation. A uniform 1 mho conductance is added to avoid numerical divergence. In addition to the Gaussian distribution in the midnight sector which is applied to case 1, the input conductivities in cases 2–11 include a combination of Gaussian distributions in the morning and afternon sectors. This modification is inspired by the observations (Ahn, 1983; Wallis and Budzinski, 1981) showing that the conductivity peaks not only in the midnight sector, but also in the morning and afternoon sectors. A theoretical study shows that a high density diffuse aurora precipitation driven by convection in the plasma sheet can extend towards the noon sector (Fontaine and Blanc, 1983).

In cases 2 through 8 the ratio of Σ_H/Σ_P is 1.5, while in cases 9, 10 and 11 the ratios vary between 0.5 and 2.0.

Figure 1 shows the input parameters common to all the cases studied in this paper. The ionospheric projection of the input magnetospheric convection pattern is shown in the top panel. The assumed distribution of the magnetospheric reflection coefficient R_m shown in the bottom panel is based on equation (2).

Figure 2(A) shows the input ionospheric conductivity model of case 2. The conductivity due to the diffuse aurora precipitation in the morning and the afternoon sectors has a 15 mho maximum around 05:00 M.L.T. and around 19:00 M.L.T. at 67° latitude, respectively, and extends toward the noon sector along the auroral oval. They are Gaussian distributions with 3° latitudinal width and 60° longi-

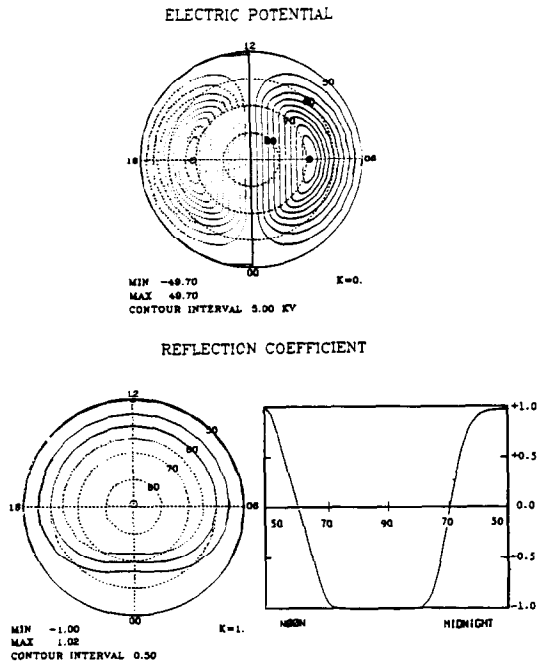

FIG. 1. THE TOP PANEL IS THE INPUT POTENTIAL PATTERN, THE BOTTOM PANELS ARE CONTOURS OF THE REFLECTION COEFFICIENT IN THE MAGNETOSPHERE (LEFT) AND ITS LATITUDINAL DEPENDENCE ALONG THE NOON–MIDNIGHT MERIDIAN (RIGHT).

tudinal. The results are shown in panels (B)–(F). Panel (B) shows the resulting convection pattern. It is similar to that in Kan and Sun (1985) in which the distortion is most noticeable near the Harang discontinuity region. Panel (C) shows the distribution of the field-aligned currents after 10 bounces of Alfvén waves in this case. The ratio of the peak intensity of the Region II current to that of Region I current is about 0.43 in this case. The most intense Region II current occurs between 21:00 and 23:00 M.L.T. in the afternoon sector and between 03:00 and 06:00 M.L.T. in the morning sector. The Region II field-aligned current in this case is in good agreement with observations (Iijima and Potemra, 1978). Panels (D) and (E) show the Hall conductance and ionospheric electrojet currents. Panel (F) shows the resulting Joule heat production rate. It is in good agreement with that estimated by Ahn and Akasofu (1983).

Figure 3 shows the results of case 3 in the same format as Fig. 2. The longitudinal gradient of the conductivity in the morning and afternoon sectors in this case is a factor of 2 smaller than that in case 2. The results show that the Region II field-aligned current density decreases with decreasing conductivity gradient.

Figure 4 shows the results of case 4. In this case the conductivity extends toward the noon sector along the auroral oval only in the afternoon sector. The peak value of the conductivity in the afternoon sector is 22.5 mho. As we can see from the results of this case, the Region II current in the morning sector is very weak due to the decrease of the conductivity; the Joule heat production rate and the westward electrojet in the morning sector are also reduced.

Figure 5 shows the results of case 5. In contrast to case 4, the conductivity in case 5 as shown in panel (A) extends toward the noon sector only in the morning sector. The peak value of the conductivity in the morning sector is 22.5 mho. This change of the conductivity resulted in a significant increase of the Region II current in the morning sector as shown in panel (C). The ratio of the peak intensity of the Region II current to that of the Region I current is 0.48. Meanwhile the electric field in the morning sector is reduced. The maximum value of the Joule heat production rate in this case jumped to 16.6 mW m^{-2} which is significantly higher than these in cases (2)–(4). The westward electrojet in the morning sector is also more intense than that in case 2.

Figure 6 shows the results of case 6. The conductivity in the morning and afternon sector is shifted 5° equatorward from its position in case 2. The Region II field-aligned current is much reduced as compared with case 2. The peak value of the Region II current to that of Region I is about 0.32.

Figure 7 shows the results of case 7. The input conductivity in the morning and afternoon sectors in panel (A) is shifted 5° poleward from its position in case 2. The Region II field-aligned current becomes even weaker than in case 6. The ratio of the peak value of Region II current to that of Region I current dropped to about 0.27. The maximum of the Joule heat production rate decreased to 7.9 mW m^{-2}.

Figure 8 shows the results of case 8. The input conductivity in this case is same as in case 2 except adding a conductivity distribution in the noon sector as shown in (A). The resulting field-aligned currents appear to rotate counterclockwise in this case and become more intense in the noon sector and weaker in the midnight sector than those in case 2.

Figure 9 shows the results of case 9. The input Hall conductivity is identical to that in case 2 except the ratio Σ_H/Σ_P is reduced to 0.5. Comparing with the results in case 2, we see that (i) the distortion of the convection pattern in the Harang discontinuity region is reduced, (ii) the Region II field-aligned current is reduced, (iii) the southward component of the west-

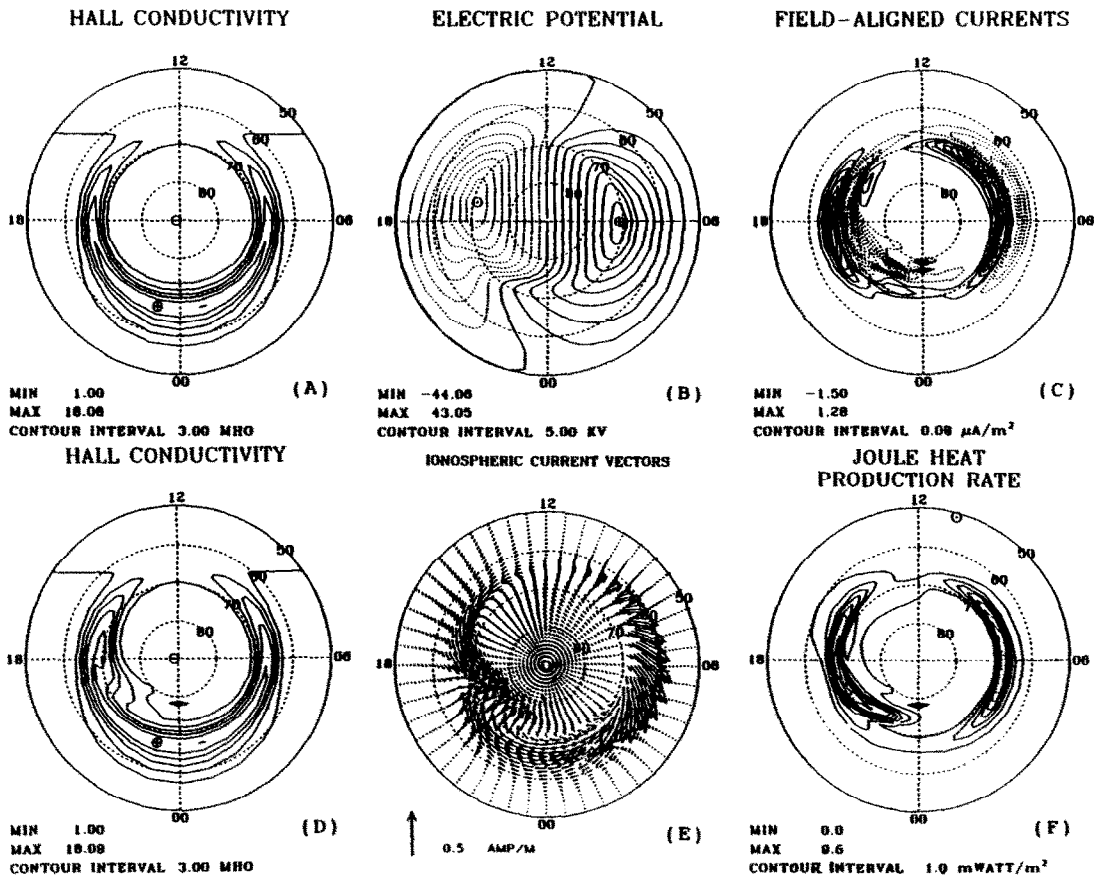

FIG. 2. THE INPUT CONDUCTIVITY EXTENDING TO NOON SECTOR IS SHOWN IN (A). (B)–(F) are the results after 10 bounces of Alfvén waves.

ward electrojet in the morning sector is strengthened and (iv) the Joule heat production rate is almost doubled.

Figure 10 shows the results of case 10. The input Hall conductivity is identical to that in case 2, except the ratio Σ_H/Σ_P is increased to 2.0. The distortion of the convection pattern in this case is the greatest among all our cases while the Region II field-aligned current, the South component of the westward electrojet in the morning sector and the Joule heat production rate are reduced as compared with those in case 2.

Figure 11 shows the results of case 11. The input Hall conductivity is the same as in case 2 except the ratio $\Sigma_H/\Sigma_P = 0.5$ in the morning and afternoon sectors while $\Sigma_H/\Sigma_P = 2.0$ in the midnight sector. It can be seen that the resulting ionospheric currents are more intense in the morning and afternoon sectors than in case 2. The ratio of the peak value of the Region II current to that of the Region I current is about 0.59 in the morning sector and 0.57 in the afternoon sector.

Table 1 summarizes the dependence of the Region II currents on the ionospheric conductivity. It is seen that case 5, case 9 and case 11 have greater Region II field-aligned current than other cases. From case 2 and case 3 we can see that the gradients of the conductivity in the morning and afternoon sectors are the dominant factor controlling the Region II current density. Case 4 and case 5 show that the Region II field-aligned current is much more sensitive to the conductivity in the morning sector than the afternoon

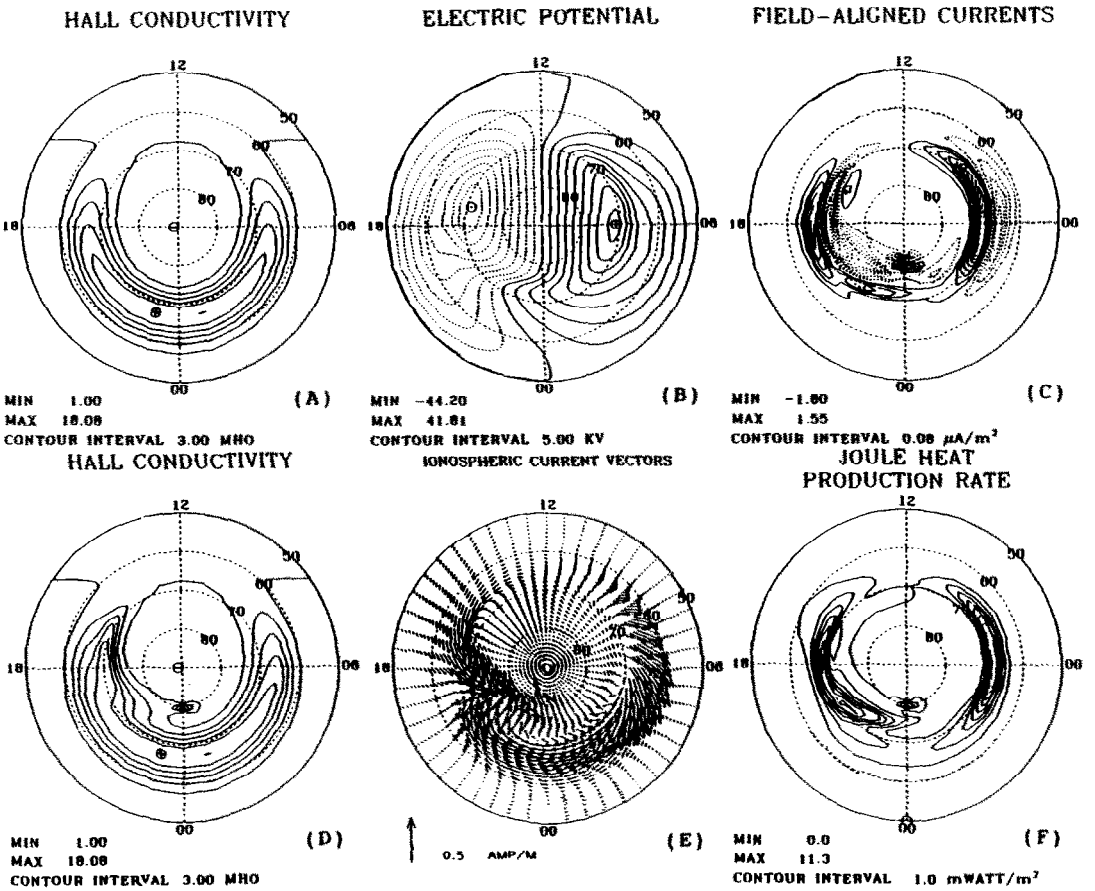

FIG. 3. THE INPUT CONDUCTIVITY WITH LOWER LONGITUDINAL GRADIENT IS SHOWN IN (A). (B)–(F) are the results after 10 bounces of Alfvén waves.

TABLE 1. SUMMARY OF CASES

Case	Hall conductivity, Peak value (mho) Midnight	Morning	Afternoon	Σ_H/Σ_P	Character	$J_{\parallel\max}$(II)/$J_{\parallel\max}$(I) Morning	Afternoon
1*	15	0	0	1.5	Night sector only	0.14	0.32
2	15	15	15	1.5	Typical case	0.38	0.42
3	15	15	15	1.5	Lower gradient	0.33	0.30
4	15	0	22.5	1.5	Weak in morning sector	0.10	0.49
5	15	22.5	0	1.5	Weak in afternoon sector	0.54	0.48
6	15	15	15	1.5	Equatorward shift	0.40	0.26
7	15	15	15	1.5	Poleward shift	0.10	0.27
8	15	15	15	1.5	Intense in noon sector	0.40	0.35
9	15	15	15	0.5	Same as case 1	0.50	0.53
10	15	15	15	2.0	Same as case 1	0.38	0.38
11	15	15	15	0.5/2.0	Same as case 1	0.59	0.57

* Kan and Sun case.

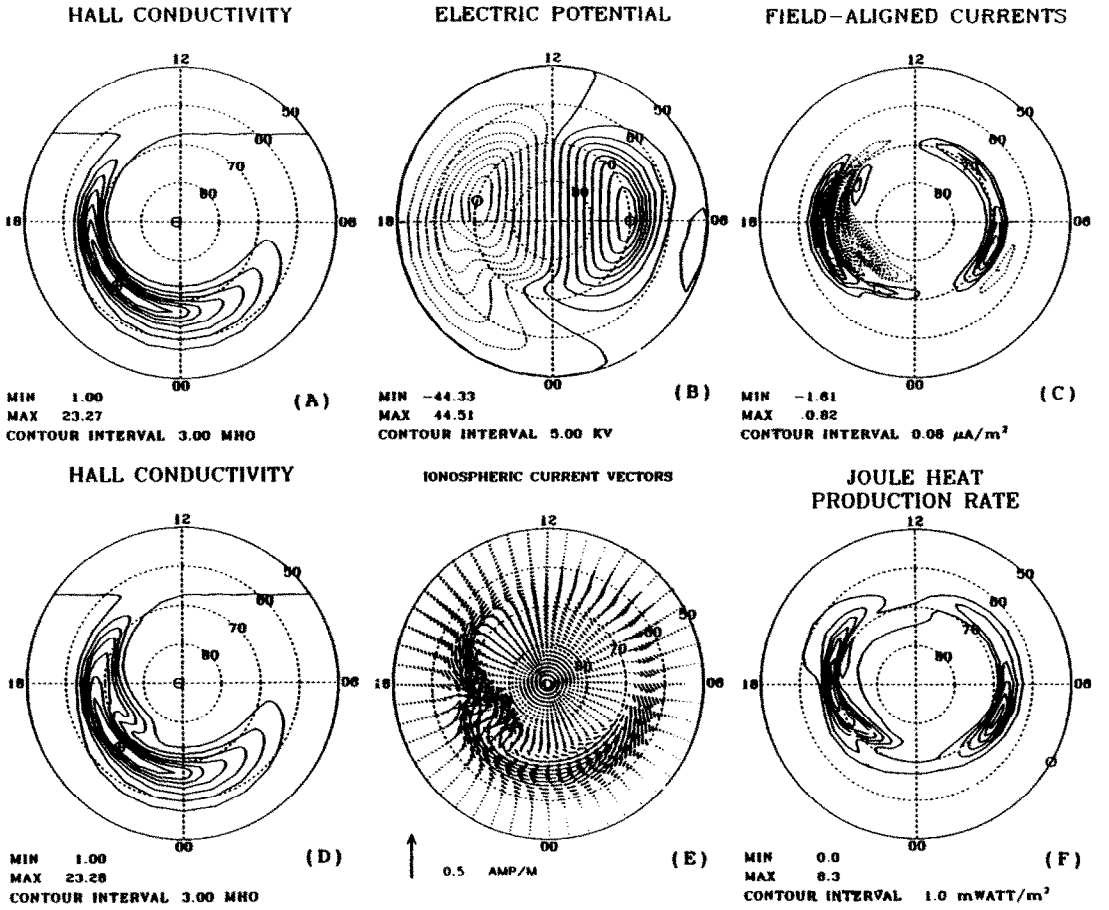

FIG. 4. THE UNSYMMETRIC INPUT CONDUCTIVITY WITH PEAK VALUE IN THE AFTERNOON SECTOR IS SHOWN IN (A). (B)–(F) are the results after 10 bounces of Alfvén waves.

sector. Comparing the last two cases we see that for the same Hall conductivity the Region II current increases with increasing Pedersen conductivity.

3. SUMMARY

We have conducted a systematic numerical study of the dependence of the Region II currents on the ionospheric conductance. The results show the following.

(1) The Region II field-aligned current density increases with increasing latitudinal gradient of the ionospheric conductance in the morning and afternoon sectors along the auroral oval. The extension of the conductivity deep into the dayside around the auroral oval is required to produce the Region II field-aligned current with the observed characteristics. The conductivity produced by the diffuse aurora in the afternoon sector is less important than its counterpart in the morning sector for the Region II field-aligned current because the conductivity in the afternoon sector is strongly enhanced by the discrete auroral precipitation during substorms.

(2) The Region II field-aligned current is found to increase as the conductivity ratio Σ_H/Σ_P is reduced by increasing Σ_P.

(3) The electric field in the ionosphere is reduced in the high conductivity region and increased in the nearby low conductivity region causing the convection pattern to penetrate to lower latitudes. In other words, high conductivity in the morning and afternoon sectors tends to force the convection to penetrate to lower latitude and, at the same time, enhance the Region II field-aligned current.

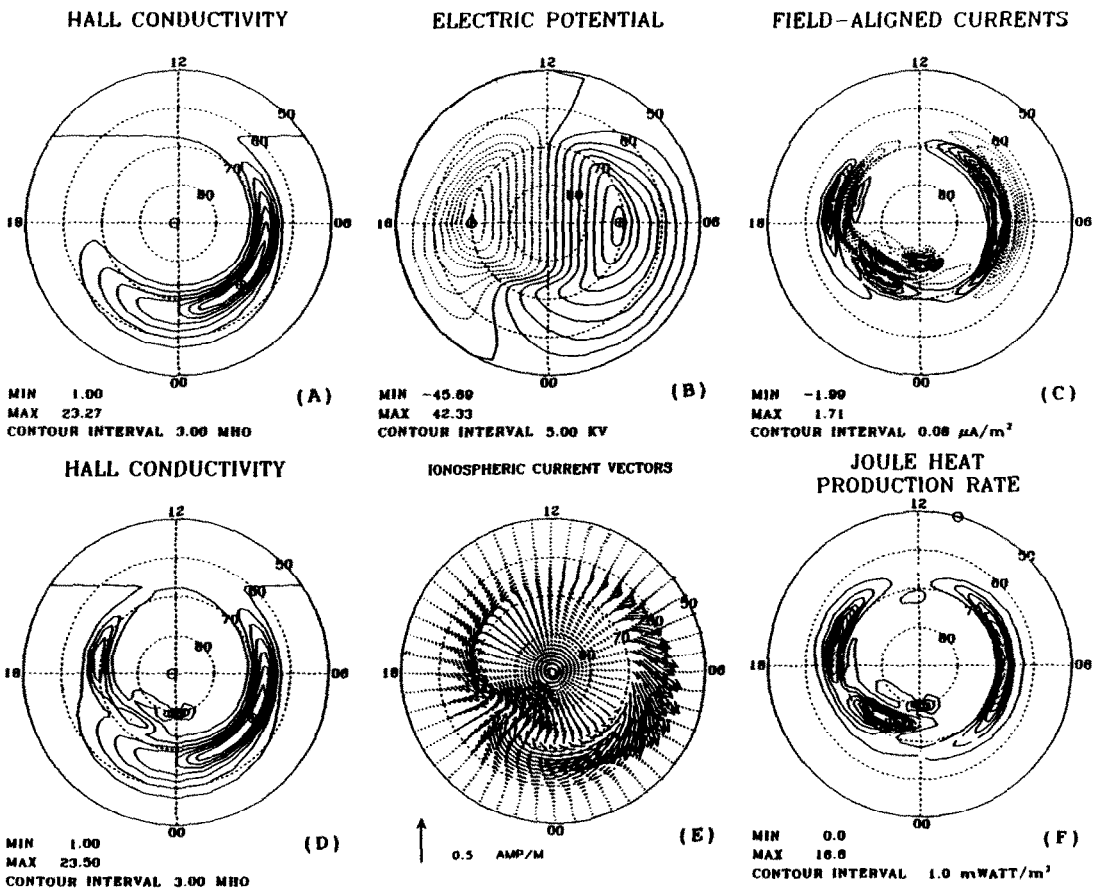

FIG. 5. THE UNSYMMETRIC INPUT CONDUCTIVITY WITH PEAK VALUE IN THE MORNING SECTOR IS SHOWN IN (A). (B)–(F) are the results after 10 bounces of Alfvén waves.

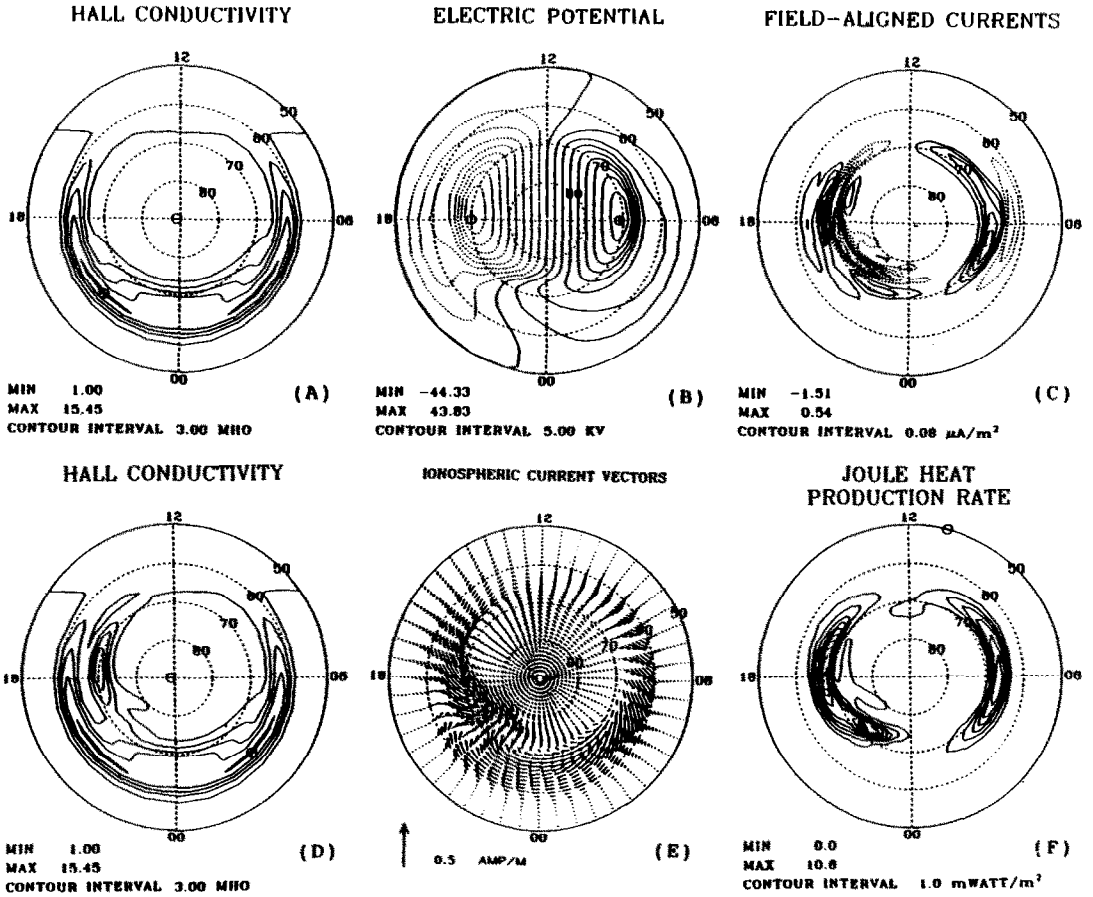

FIG. 6. THE INPUT CONDUCTIVITY SHIFTED EQUATORWARD IN THE MORNING AND AFTERNOON SECTORS IS SHOWN IN (A).
(B)–(F) are the results after 10 bounces of Alfvén waves.

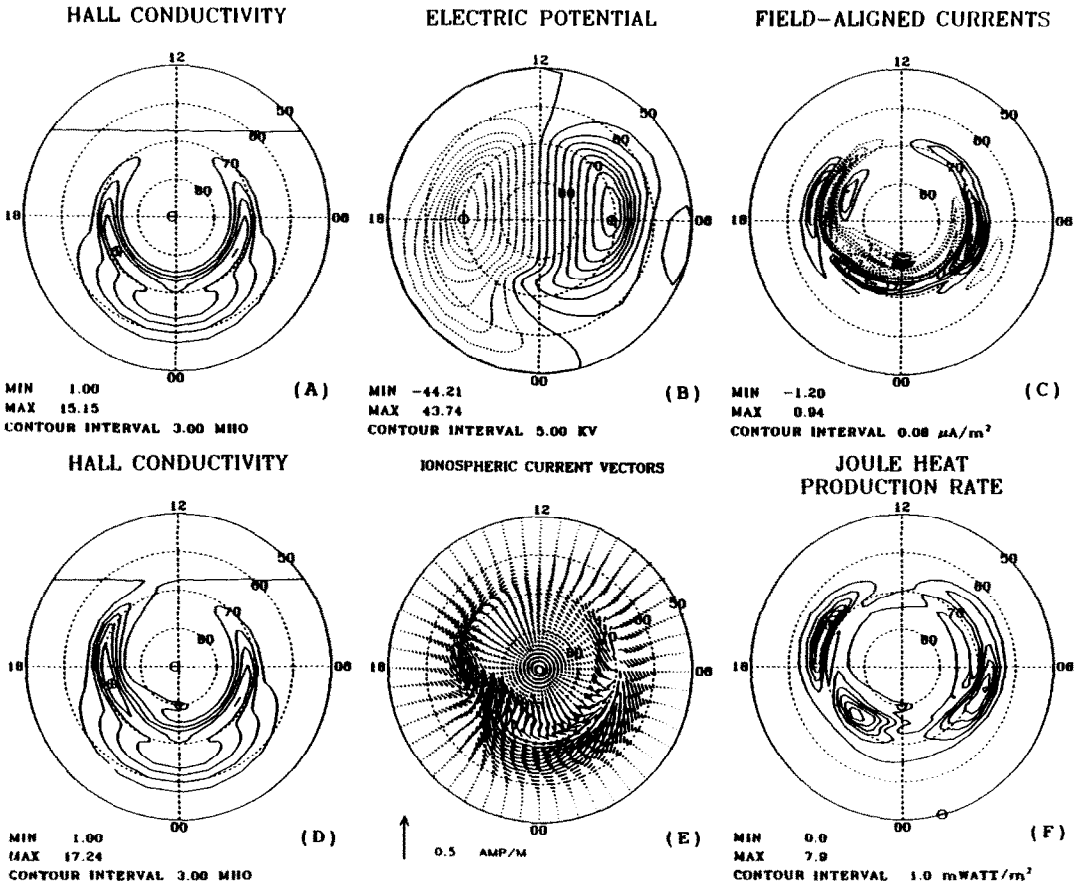

FIG. 7. THE INPUT CONDUCTIVITY SHIFTED POLEWARD IN THE MORNING AND AFTERNOON SECTORS IS SHOWN IN (A).
(B)–(F) are the results after 10 bounces of Alfvén waves.

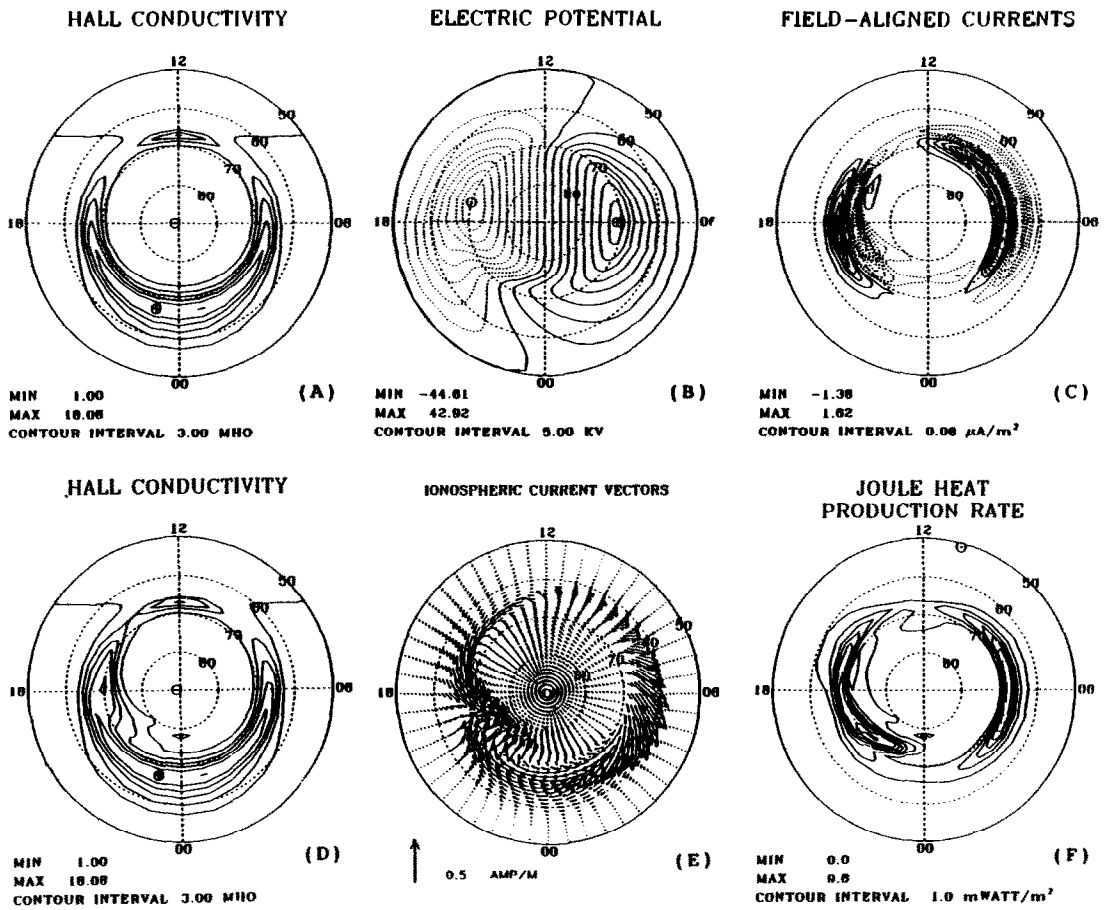

FIG. 8. THE INPUT CONDUCTIVITY WITH AN INTENSE PART IN THE NOON SECTOR IS SHOWN IN (A). (B)–(F) are the results after 10 bounces of Alfvén waves.

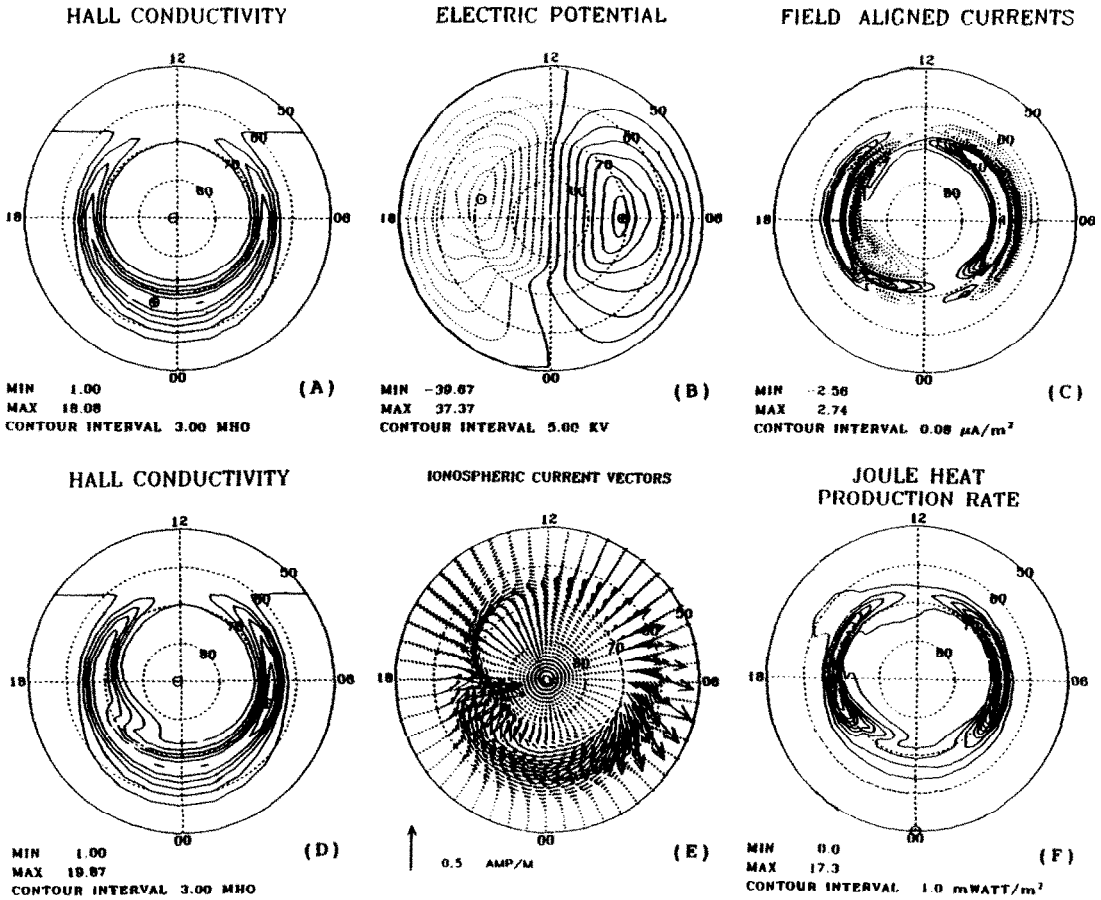

FIG. 9. THE CASE WITH THE INPUT CONDUCTIVITY RATIO $\Sigma_H/\Sigma_P = 0.5$.
The input Hall conductivity shown in (A) is the same as in Fig. 2(A). (B)–(F) are the results after 10 bounces of Alfvén waves.

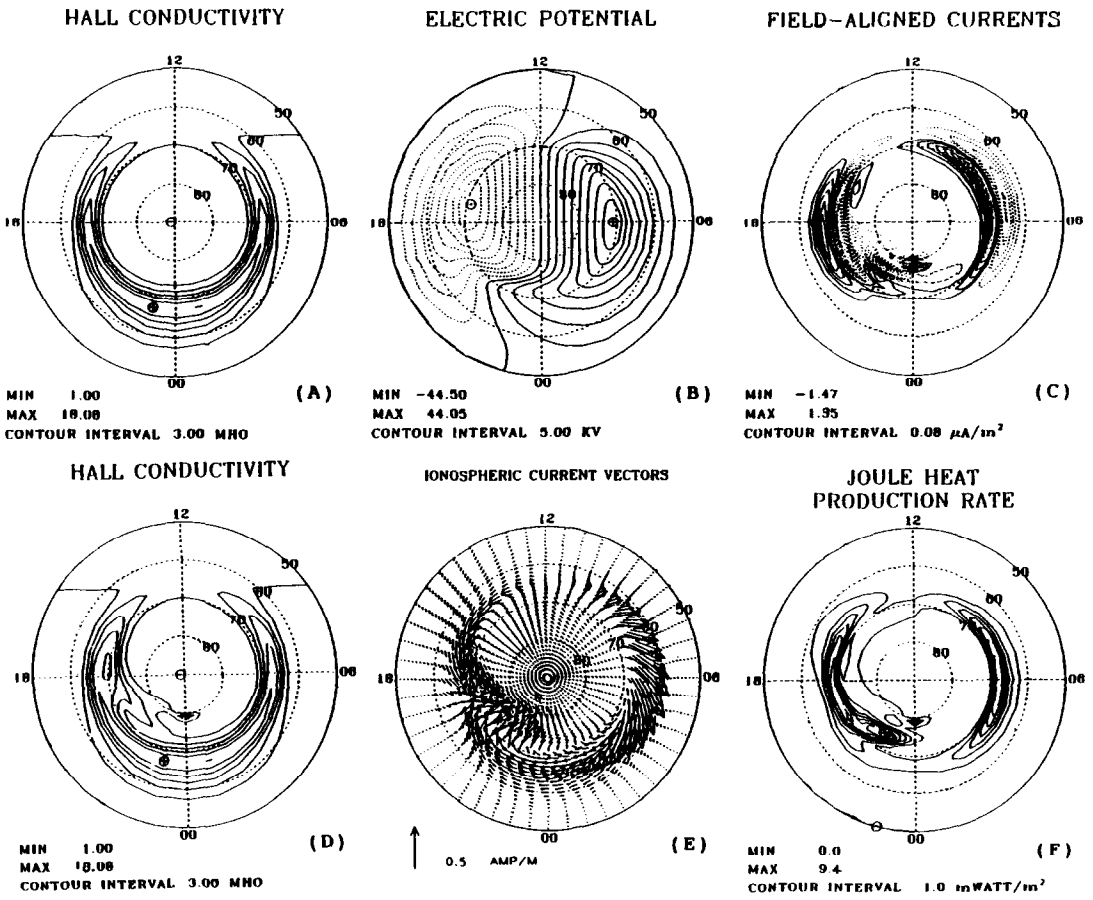

FIG. 10. THE CASE WITH THE INPUT CONDUCTIVITY RATIO $\Sigma_H/\Sigma_P = 2.0$.
The input Hall conductivity shown in (A) is the same as in Fig. 2(A). (B)–(F) are the results after 10 bounces of Alfvén waves.

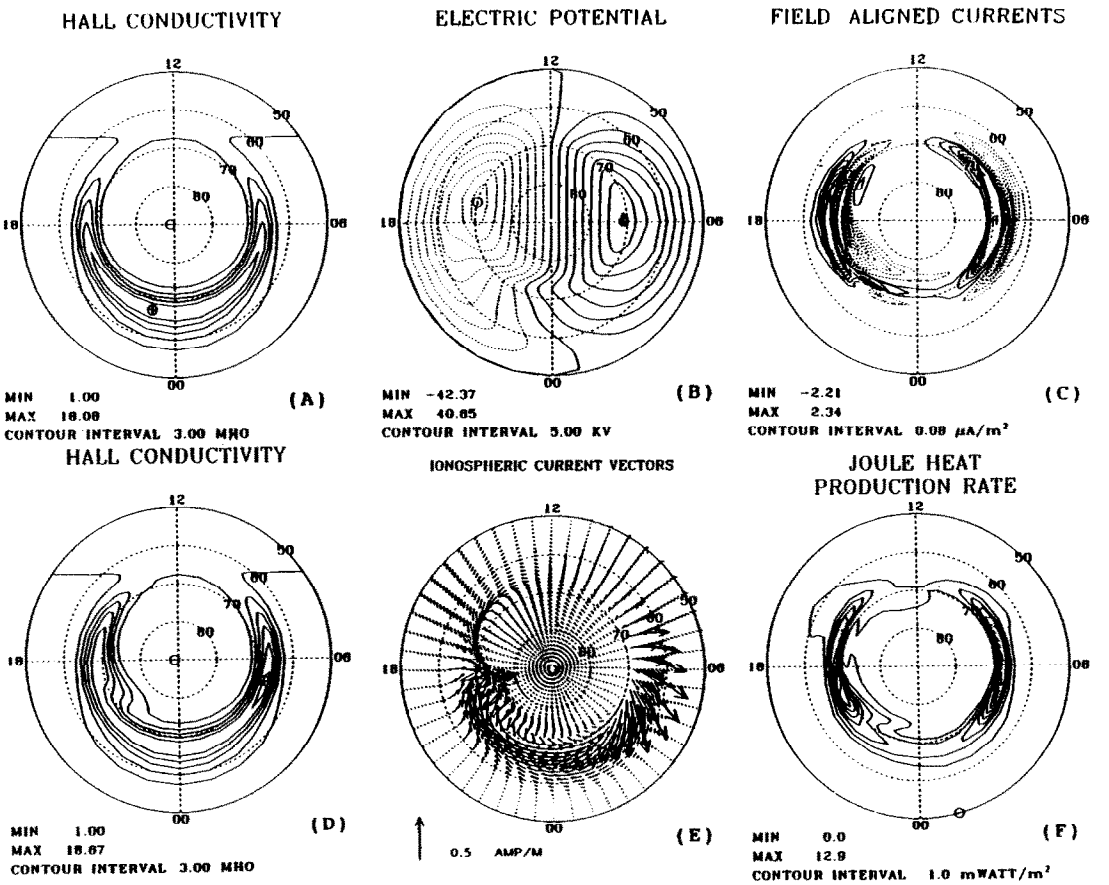

FIG. 11. THE CASE WITH THE INPUT CONDUCTIVITY RATIO $\Sigma_H/\Sigma_P = 0.5$ IN THE MORNING AND AFTERNOON SECTORS, $\Sigma_H/\Sigma_P = 2.0$ IN THE MIDNIGHT SECTOR.
The input Hall conductivity shown in (A) is the same as in Fig. 2(A). (B)–(F) are the results after 10 bounces of Alfvén waves.

(4) The Joule heat production rate calculated in the model is in reasonable agreement with that estimated from the observations (Ahn and Akasofu, 1983).

Acknowledgements—This work was supported in part by NSF grants ATM85-21194 and ATM85-01718.

REFERENCES

Ahn, B.-H. (1983) Electric conductivities, currents and energy dissipation in the polar ionosphere. Ph.D. thesis, University of Alaska.

Ahn, B.-H. and Akasofu, S.-I. (1983) The joule heat production rate and the particle energy injection rate as a function of the geomagnetic indices *AE* and *AL*. *J. geophys. Res.* **88**, 6275.

Fontaine, D. and Blanc, M. (1983) A theoretical approach to the morphology and the dynamics of diffuse auroral zones. *J. geophys. Res.* **88**, 7171.

Iijima, T. and Potemra T. A. (1978) Large-scale characteristics of field-aligned currents associated with substorms. *J. geophys. Res.* **83**, 599.

Kan, J. R. and Kamide, Y. (1985) Electrodynamics of the westward traveling surge. *J. geophys. Res.* **90**, 7615.

Kan, J. R. and Sun, W. (1985) Simulation of the westward traveling surge and Pi2 pulsations during substorms. *J. geophys. Res.* **90**, 10911.

Sugiura, M., Iyemori, T., Hoffman, R. A., Maynard, N. C., Burch, J. L. and Winningham, J. D. (1984) Relationships between field-aligned currents, electric field, and particle precipitation as observed by *Dynamics Explorer*-2, in *Magnetospheric currents*, Geophys. Monogr. Ser. Vol. 28 (Edited by Potemra, T. A), p. 96. AGU, Washington, DC.

Sugiura, M. and Potemra, T. A. (1976) Net field-aligned currents observed by *TRIAD*. *J. geophys. Res.* **81**, 2155.

Wallis, D. D. and Budzinski, E. E. (1981) Empirical models of height-integrated conductivities. *J. geophys. Res.* **86**, 125.

Zmuda, A. J. and Armstrong, J. C. (1974) The diurnal flow pattern of field-aligned currents. *J. geophys. Res.* **79**, 4611.